Microscopic Analysis of Large-Cluster Explosion in Intense Laser Fields

Christian Jungreuthmayer,[1] Michael Geissler,[2] Jürgen Zanghellini,[1] and Thomas Brabec[1,*]

[1]*Center for Photonics Research, University of Ottawa, 150 Louis Pasteur, Ottawa, Ontario, Canada K1N 6N5*

[2]*Max-Planck-Institut für Quantenoptik, Hans-Kopfermann-Strasse 1, D-85748 Garching, Germany*

(Received 18 August 2003; published 30 March 2004)

We present a three dimensional microscopic particle in cell code. The code models nanoplasmas in intense laser fields, taking account of all relevant microscopic interactions. Our simulation reveals the physical processes determining the laser induced explosion of large clusters with several 10 000 atoms.

DOI: 10.1103/PhysRevLett.92.133401 PACS numbers: 36.40.Vz, 36.40.Gk, 52.50.Jm

Atomic clusters exposed to intense laser pulses explode and create a hot, dense plasma [1]. This process is of interest for the generation of x rays [2], for electron and ion acceleration [3], and for the creation of nuclear particles [4]. For the design of such experiments, a thorough understanding of the cluster explosion dynamics is essential.

In small clusters, containing a few 100 atoms, laser heated electrons can escape easily. The positive space charge of the remaining ions leads to Coulomb explosion. Small clusters are accessible to molecular dynamics (MD) simulations [5–8]. As a result, their explosion dynamics is relatively well understood. In clusters with more than 1000 atoms the situation becomes more complicated. MD simulations are limited to about $N = 1000$ atoms [9], because the workload increases with N^2. Therefore, analysis of the explosion of large clusters relies on phenomenological models [10,11]. Currently, there are no numerical methods that can properly take into account both, microscopic and hydrodynamic, macroscopic phenomena. As a result, the physical mechanisms determining the explosion of large clusters could not be identified unambiguously so far.

In this Letter we introduce a 3D microscopic particle in cell (MPIC) code that takes account of all important microscopic effects in the evolution of laser driven, large clusters. Regular particle in cell (PIC) codes [12,13] solve the Maxwell equations and the relativistic classical equations of motion on a stationary grid using the mean field approximation. The charged particles are represented by boxes with macroscopic dimensions that represent the average over many particles. As a result, microscopic effects such as inverse bremsstrahlung heating, impact ionization, electron-electron scattering, electron-ion scattering, and charge enhanced ionization (CEI) [7] cannot be taken into account. In the MPIC code the box size is shrunk to the order of 1 a.u. containing only one charged particle. In this limit, the microscopic interactions of all charged particles are taken care of by the PIC formalism [14].

The MPIC code contains no free parameters and presents a virtual experiment. To test its reliability we have calculated recent experiments reporting an asymmetric explosion of Ar and Xe clusters [15,16] with $N \geq 10\,000$. The calculated spectra and angular distributions of electrons and ions are found to be in good agreement with experiments.

The MPIC simulations reveal the first complete picture of the explosion of large clusters. The essential new findings are as follows: (i) The explosion is driven by a combination of electrostatic (Coulomb explosion) forces [17] and hydrodynamic processes [10,11]. Our analysis does not confirm resonant laser plasma coupling predicted by hydrodynamic models [10,11]. (ii) CEI plays a major role in the Coulomb explosion of molecules [18,19] and small clusters [7]. CEI and a related mechanism dubbed polarization enhanced ionization (PEI) dominate the ionization process in large clusters, too. PEI also explains the asymmetric explosion observed in recent experiments [15,16]. (iii) The main electron heating mechanism is laser dephasing heating (LDH). The macroscopic, electric field of the cluster causes dephasing between the laser driven motion of the electrons and the laser field which allows electrons to absorb energy from the laser.

The MPIC code calculates the classical dynamics of all charged particles. Quantum mechanical phenomena, such as ionization, have to be added. The ionization of atoms and ions [7] is calculated by using the ADK (Ammosov-Delone-Krainov) tunneling rate [20]. The MPIC code solves the Maxwell equations and calculates the complete electromagnetic field of the laser and of all charged particles in the whole simulation volume at each time step. The value of this field at the position of the individual atoms/ions, E, is inserted into the ADK theory and yields the ionization probability. The actual ionization events are calculated from the ADK rates by using a Monte Carlo technique. The ionized electron is born by putting the center of gravity of the corresponding box a distance I_p/E away from the ion, along the direction of the electric field vector. At this point the tunneling electron wave packet penetrates the barrier. Here, I_p is the ionization potential. The electron velocity at the time of birth is assumed to be zero. Further, impact ionization is taken into account by the Lotz formula [8,21]. The MPIC code makes and continuously updates a map of all ion positions, similar to the linked list method in MD

simulations [22]. The map is used to determine the nearest ions surrounding each electron. Impact ionization occurs whenever a free electron moves into the area around an ion determined by the Lotz cross section. Tunnel ionization is disabled as long as the electron is within this area. Finally, all other microscopic effects can, to a good approximation, be treated classically and are taken account of by the MPIC formalism.

Our analysis is performed for the parameters of recently published experiments [15,16]. The neutral cluster is modeled by atoms at rest that are arranged in an fcc lattice. However, the choice of the initial condition is uncritical, as the explosion of large clusters is dominated by the macroscopic dynamics of the nanoplasma. The experiments are performed in the limit of low cluster density, where the interaction between neighboring clusters is negligible. The length of the simulation box is chosen 5 times the cluster diameter, and open boundary conditions are used. The particles leaving the simulation volume before the end of the laser pulse have to be postprocessed, in order to determine the ion and electron spectra. This is done by using a mean field PIC approach outside the simulation volume. The laser pulse propagates in the z direction and is linearly polarized in the x direction. The pulse duration is 100 fs and the peak intensity 8×10^{15} W/cm^2. We have calculated an Ar cluster with 10 000 atoms and a Xe cluster with 25 000 particles. The cluster diameters are 9 and 14 nm, and the interatomic distances are 0.375 and 0.434 nm, respectively. The size of the box representing one particle (atom, ion, electron) is 0.1 nm. The calculations were performed on 16 SUN Ultra Sparc III processors and took 23 days for the $Ar_{10\,000}$ cluster.

The ion spectrum in Fig. 1(a) was calculated for an $Ar_{10\,000}$ cluster. In the low energy range the ion spectra in and perpendicular to the laser polarization coincide. In the cutoff region, for energies greater than 2×10^4 eV, the spectra differ. Ions emitted along the laser electric field are shifted to higher energies in agreement with the experiments reported in [15]. The 16 processors were not sufficient to calculate an $Ar_{40\,000}$ cluster to make a quantitative comparison with Ref. [15]. However, we could calculate the electron spectrum of the $Xe_{25\,000}$ cluster experiment in [16] by choosing a larger box size of 0.15 nm. The exponentially decaying part of the spectrum in Fig. 1(b) can be described by a single temperature that is 800 eV. This is slightly higher than the 700 eV measured in Ref. [16]. The good agreement demonstrates the predictive power of the MPIC code.

The essential elements of the cluster explosion dynamics can be understood from Fig. 2. Our calculation shows that ionization is dominated by field ionization, and collisional ionization is negligibly small during the whole cluster explosion, in agreement with conclusions obtained from small cluster simulations [8]. Figure 2(a1) shows a snapshot of the ion charge states at the leading edge of the laser pulse, where the laser intensity is

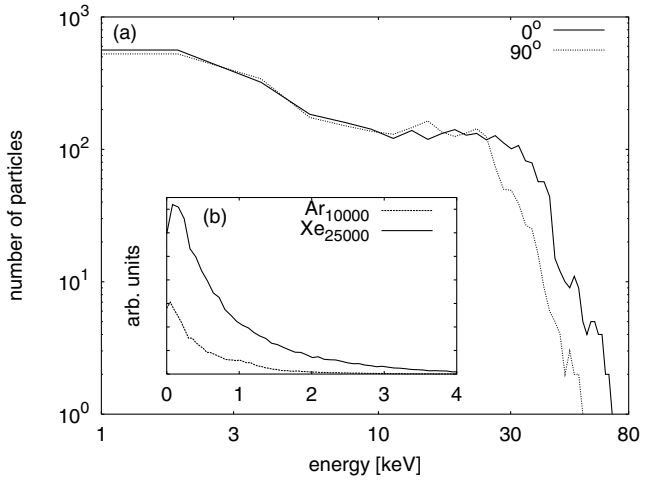

FIG. 1. (a) Energy spectra of ions emitted by an $Ar_{10\,000}$ cluster after irradiation with an 100 fs FWHM (full width at half maximum) laser pulse, $\sin^2$ pulse envelope, peak intensity $I = 8 \times 10^{15}$ W/cm^2, wavelength $\lambda = 800$ nm. The laser field propagates in the z direction and is linearly polarized in the x direction. The solid and dotted lines refer to ion emission parallel and perpendicular to the laser electric field. (b) Electron energy spectrum for $Ar_{10\,000}$ and $Xe_{25\,000}$. The exponentially decaying part of the spectrum can be described by a single temperature that is 600 and 800 eV for the Ar and the Xe cluster, respectively.

4.4×10^{14} W/cm^2. Singly and doubly charged ions are created in the cluster core. This is at first sight surprising, as the laser intensity is too small for the creation of doubly charged ions. The mechanism becomes clear by inspecting the electric field in the cluster, depicted in Fig. 2(a3). Electrons are heated and leave the cluster. The heating mechanism is discussed below. The net positive charge of the excess ions gives rise to the buildup of an electric field. Electron density fluctuations locally increase the field strength to values comparable to laser intensities of 10^{15} W/cm^2. The electric field causes CEI, similar to CEI in molecules [18,19], however, with an additional stochastic component. Similar mechanisms might also play a role in the ionization and damage of dielectric materials.

Figures 2(a1), 2(a2), and 2(a3) reveal another ionization mechanism related to CEI. The red spots in Fig. 2(a1) indicate enhanced ionization at the cluster poles. The enhanced ionization originates in the laser induced polarization of the electron cloud. The laser field is strong enough to push the electron cloud over the cluster boundary, as depicted in Fig. 2(a2). As a result, an electric field is generated at the opposite pole of the cluster by electron depletion, see Fig. 2(a3). The polarization induced electric field at the poles exceeds the laser electric field by up to an order of magnitude, and causes PEI. PEI is responsible for the creation of the highest charge states and creates the high energy end of the ion spectrum. The different ionization states at the poles and at the equator are responsible for the asymmetric ion spectrum in Fig. 1.

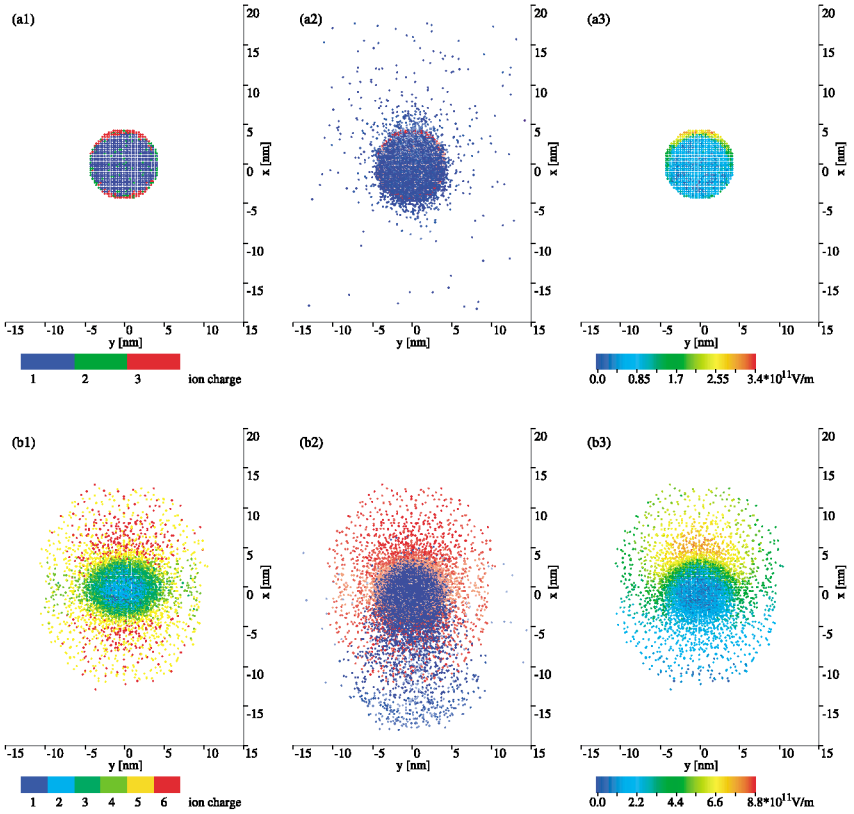

FIG. 2 (color). This figure shows the x-y plane going through the cluster center: (1) charge state of ions versus position; (2) position of ions (red dots) and electrons (blue dots); (3) electric field at the position of the ions for the parameters of Fig. 1. (a) and (b) refer to the times of observation $t = -92.9$ fs, -25.9 fs, where $t = 0$ marks the peak of the laser pulse. The laser intensities for (a) and (b) are $I = 4.4 \times 10^{14}$ W/cm^2 ($E = 5.7 \times 10^{10}$ V/m) and $I = 6.7 \times 10^{15}$ W/cm^2 ($E = 2.2 \times 10^{11}$ V/m), respectively.

With increasing time more electrons are heated and escape the cluster. In contrast to Fig. 2(a2), where the electrons are still evenly distributed over the cluster core, the remaining bound electrons in Fig. 2(b2) are no longer sufficient to shield the whole cluster. As a result, only the center of the cluster is shielded, and the electron density drops to zero towards the cluster surface. The reduced electron shielding towards the cluster surface creates an ion electric field, which is represented by the green ring in Fig. 2(b3). The ion electric field dominates the laser field, however, it is weaker than the field at the cluster poles. It causes CEI, creating the green colored shell of higher charged ions around the cluster center in Fig. 2(b1). The resulting positive space charge ejects ions symmetrically from the cluster and creates the intermediate energy ions in Fig. 1.

The cluster core keeps its shape and size over a significant fraction of the laser pulse; see Figs. 2(b1) and 2(b2). The reason is that due to electron shielding the positive space charge in the cluster core is kept small. After the peak of the laser pulse, no new electrons are created by ionization. The continuous ejection of hot electrons starts to deplete the cluster center. As a result, the ion core starts to expand, further facilitating the escape of the remaining electrons. The cluster is completely depleted of electrons 50 fs after the laser pulse peak. In the absence of electrons CEI takes place again, creating charge states up to 3+ in the cluster center. The cluster center undergoes symmetric Coulomb explosion and forms the low energy part of the ion spectrum in Fig. 1.

There has been an ongoing discussion of whether hydrodynamic pressure or electrostatic forces drive the explosion of large clusters [10,11,17]. Which of the two mechanisms prevails depends on the rate at which electrons are heated and can leave the cluster. Our MPIC simulations reveal that all electrons are removed from the cluster. However, in contrast to small clusters, where all electrons are emitted at early stages, electrons in large clusters are removed gradually. Depletion starts at the cluster boundary and then gradually progresses towards the center. As a result, the explosion dynamics is determined by an interplay between electrostatic forces (Coulomb explosion and CEI) and plasma processes which shield parts of the cluster.

A surprising element of our simulations is that all electrons are heated sufficiently to leave the cluster core. Inverse bremsstrahlung can be ruled out as the dominant electron heating mechanism. The electrons follow the laser electric field and do not exhibit an isotropic angular distribution, as would be the case for inverse

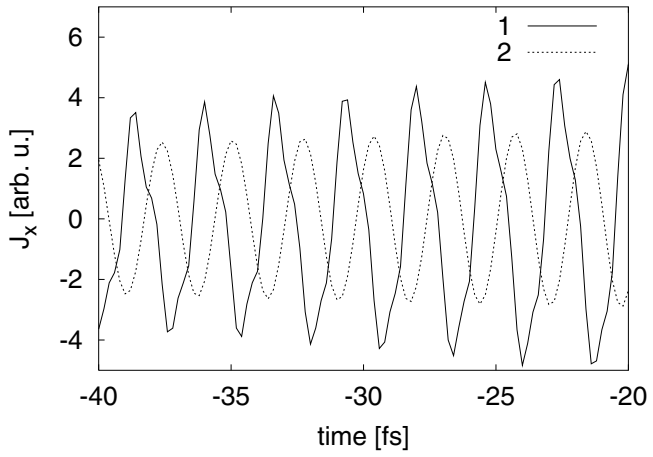

FIG. 3. This figure shows the macroscopic electron current J_x (1), as defined in the text, and the current of a single free electron (2) in the direction of the laser electric field. The currents were scaled to a similar size to facilitate comparison. The phase difference between a free electron current and a cluster current and the nonsinusoidal (nonlinear) contributions (corresponding to higher harmonics of the laser field) lead to laser dephasing heating (LDH) of the electrons.

bremsstrahlung heating. We have identified LDH as the dominant mechanism. Electron energy absorption is determined by the integral $L = \int \mathbf{J}\mathbf{E}dt = \int J_x E_x dt$. The electron current in the direction of the laser electric field is determined by the sum over all electrons, $J_x = dP_x/dt = e\sum_i dx_i/dt\delta(\mathbf{r} - \mathbf{r}_i)$, where e is the electron charge, P_x is the polarization in the x direction, $\mathbf{r}_i$ is the position vector of the ith electron, and x_i its x component. For free electrons, $dx/dt = \int_{-\infty}^{t} E_x(t')dt'$, and the cycle averaged energy absorption is zero. During the intense laser cluster interaction a macroscopic charge and electric field gradient builds up in and around the cluster, see Figs. 2(b1) and 2(b3). The resulting electric field leads to dephasing between laser field and polarization, and to nonlinear polarization terms; see Fig. 3. Both effects result in nonzero contributions to the cycle averaged integral L and therewith cause LDH. Note that the basic mechanism of LDH is related to inverse bremsstrahlung. However, whereas in inverse bremsstrahlung, energy absorption is caused by the dephasing in the microscopic Coulomb field of an ion, LDH is caused by dephasing of electrons in the macroscopic electric field of the cluster.

Concluding, we have introduced a microscopic particle in cell (MPIC) code that presents a powerful tool for the analysis of nanoplasmas. We have performed calculations for clusters of up to $N = 25\,000$ atoms, taking all important microscopic interactions into account. Our simulations revealed good agreement with experiments and a complete picture of the explosion dynamics of large clusters. This progress was made possible by the fact that the numerical load of the MPIC code increases with N, whereas commonly used molecular dynamic codes scale with N^2. The calculation of nanoplasmas with up to 10^6 atoms appears feasible on large scale computers. The MPIC concept presents a first step towards an exact kinetic theory of macroscopic plasma volumes, with dimensions comparable to the (μm) laser wavelength.

The authors gratefully acknowledge invaluable discussion with J. M. Rost. This work was supported by the National Science and Engineering Research Council, Photonics Research Ontario, Canadian Institute for Photonics Innovation, and by the Austrian Science Fund, Project No. Y142-TPH.

*Email address: brabec@uottawa.ca

[1] V. P. Krainov and M. B. Smirnov, Phys. Rep. **370**, 237 (2002).
[2] A. McPherson *et al.*, Phys. Rev. Lett. **72**, 1810 (1994).
[3] Y. L. Shao *et al.*, Phys. Rev. Lett. **77**, 3343 (1996).
[4] T. Ditmire *et al.*, Nature (London) **398**, 489 (1999).
[5] C. Rose-Petruck, K. J. Schafer, K. R. Wilson, and C. P. J. Barty, Phys. Rev. A **55**, 1182 (1997).
[6] J. Kou *et al.*, J. Chem. Phys. **112**, 5012 (2000).
[7] C. Siedschlag and J. M. Rost, Phys. Rev. Lett. **89**, 173401 (2002).
[8] K. Ishikawa and T. Blenski, Phys. Rev. A **62**, 063204 (2000).
[9] I. Last and J. Jortner, Phys. Rev. A **62**, 013201 (2000).
[10] T. Ditmire, T. Donnelly, A. M. Rubenchik, R. W. Falcone, and M. D. Perry, Phys. Rev. A **53**, 3379 (1996).
[11] H. M. Milchberg, S. J. McNaught, and E. Parra, Phys. Rev. E **64**, 056402 (2001).
[12] A. Pukhov, J. Plasma Phys. **61**, 425 (1999).
[13] M. Eloy, R. Azambuja, J. T. Mendonça, and R. Bingham, Phys. Plasmas **8**, 1084 (2001).
[14] Note that in the PIC/MPIC formalism a particle is represented by a finite sized box only for the calculation of the current. For the solution of the relativistic equations of motion, particles are considered as point particles, represented by the center of gravity of their box.
[15] V. Kumarappan, M. Krishnamurthy, and D. Mathur, Phys. Rev. A **67**, 043204 (2003).
[16] V. Kumarappan, M. Krishnamurthy, and D. Mathur, Phys. Rev. Lett. **87**, 085005 (2001).
[17] M. Lezius *et al.*, Phys. Rev. Lett. **80**, 261 (1998).
[18] T. Seideman, M. Yu. Ivanov, and P. B. Corkum, Phys. Rev. Lett.**75**, 2819 (1995).
[19] T. Zuo and A. D. Bandrauk, Phys. Rev. A **52**, R2511 (1995).
[20] M. Ammosov, N. B. Delone, and V. P. Krainov, Sov. Phys. JETP **64**, 1191 (1986).
[21] W. Lotz, Z. Phys. **216**, 241 (1968).
[22] M. P. Allen and D. J. Tildesley, *Computer Simulations of Liquids* (Oxford University Press, Oxford, 2002), p. 149.